Spatiotemporal characterization of evaporated atoms during electron beam melting additive manufacturing by advanced laser diagnostics

Abderzak El Farsy, Essaid Chakib Tighidet, Charles Ballage, Tiberiu Minea

Journal of Applied Physics

AIP Publishing

Spatiotemporal characterization of evaporated atoms during electron beam melting additive manufacturing by advanced laser diagnostics

Abderzak el Farsy*, Essaid Chakib Tighidet, Charles Ballage and Tiberiu Minea

Université Paris-Saclay, CNRS, Laboratoire de Physique des Gaz et des Plasmas, 91405 Orsay, France

*Corresponding author: abderzak.el-farsy@universite-paris-saclay.fr , tiberiu.minea@universite-paris-saclay.fr

Abstract:

Electron powder bed fusion (E-PBF) is an additive manufacturing technology used to produce parts layer-wise for advanced aerospace, biomedical, and other applications. Precise control over the energy transferred to the powder by the electron beam is key to further process improvements. Here, we used tunable diode laser absorption spectroscopy to characterize the evaporated titanium atoms above the molten area of a TA6V powder alloy, and thus the effects of the energy transferred to it by the electron beam. This unconventional diagnostic tool achieves analyses at very high temporal (<1 μs) and spatial (<100 μm) resolutions, thus offering valuable information on the microsecond-scale dynamics of the micro-melting zone and on the effectiveness of the electron beam spot at diameters as small as ~200 μm. Our measurements highlighted sharp fluctuations during the evaporation process that were independent of the power and scan speed of the electron beam; instead, the molten pool surface itself seems to drive these fluctuations. Our analysis also documented the shape and density of the vapor plume, which was oriented perpendicular to the surface under common E-PBF conditions.

Keywords: metal additive manufacturing, tunable diode laser absorption spectroscopy, TA6V, dynamic of the molten pool.

I. Introduction

Electron-beam powder bed fusion (E-PBF) is an additive manufacturing (AM) processes used to print high-quality three-dimensional parts layer-by-layer.[1–3] The E-PBF market has grown exponentially over the last decade, driven mainly by advanced aerospace and biomedical applications.[4,5] The strong interest in this process is due to its operation under vacuum, improving the mechanical characteristics of the parts and obviating complex thermal post-treatments. Nonetheless, the quality of parts produced by E-PBF is directly related to the local powder melting process.

In E-PBF, a well-focused electron beam selectively melts a smooth metal powder layer, forming a molten pool.[6] Subsequent solidification of the pool transforms the metal powder into a dense solid layer. After scanning and melting one layer into the desired shape, the build table is lowered slightly, and a new powder layer is spread on the building surface. This sequence is repeated, layer-by-layer, until a complete part has been manufactured.

The electron beam's trajectory and focus are easily tuned by controlling the current passing through the electromagnetic lenses (coils). Beam scan speeds reach very high velocities, up to 10^5 m s^{-1} within the build area, meaning that the beam can jump almost instantaneously from one point to another.[3] However, the applied voltage controls the electron energy: the higher the energy, the deeper the energy deposition into the powder. Therefore, low beam power densities do not efficiently fuse the powder, whereas high power densities can result in vaporization that changes the chemical composition of the powder. The quality of the parts produced thus depends on the rapid heating and cooling phases during solidification.

Melting using a high-power electron beam leaves a distinctive deep and narrow depression in the molten material, termed a "keyhole".[7–9] This is the result of strong evaporation at the point where the focused beam delivers the highest power density. The keyhole is known to be unstable; even when using a constant and continuous electron beam, it undergoes dynamic fluctuations (Marangoni thermo-capillary convection)[10].

The development of *in-situ* measurement techniques capable of temporally characterizing the evaporation of metallic elements during E-PBF is thus crucial to ensuring the production of quality parts. Several real-time monitoring techniques aim to increase reliability and improve our understanding of the E-PBF process. Moreover, some of these diagnostics help to verify numerical simulations.[2,11] State-of-the-art *in-situ* diagnostic measurements rely on thermal imaging,[12,13] detecting thermally induced electron emissions,[14] high-speed optical imaging, optical emission spectroscopy (OES),[15–22] time-averaged tunable diode laser absorption spectroscopy (TD-LAS),[23] and laser-induced fluorescence.[24]

In our previous study[23], we reported time-averaged TD-LAS measurements demonstrating that the density of evaporated atoms is clearly related to the vapor saturation pressure. Here, we analyzed evaporated atoms during an unstable E-PBF process to reveal the spatiotemporal dynamics of the molten pool. This information gives a better understanding of the dynamics of the interaction between the electron beam and the powder, and can be used to determine optimal operating conditions for a given application. The time-evolution of the evaporated atom density reflects changes of the molten pool surface morphology, including keyhole formation, balling, etc.

Quantifying the absolute amount of metal evaporated from the molten pool is necessary to accurately predict both the instantaneous and dynamic transfer of energy to the molten pool. The measurements reported herein allowed us to reconstruct the vapor plume in the plane perpendicular to the build table; based on these reconstructions, we discuss plume dynamics under several fusion conditions.

II. Experimental setup

All measurements were *in situ* performed in a commercial General Electric ARCAM A1. Briefly, the electrons emitted from a hot tungsten filament gain 60 keV from a high-voltage acceleration field. The electron beam spot diameter on the building surface was ~200 µm. The vacuum chamber was evacuated to low pressure (2×10^{-5} Pa) before each operation, using a turbo molecular pump-based system. The printing process occurs in a Helium atmosphere fixed at 0.2 Pa. We adjusted the beam power by changing the beam current intensity within the range of 6–14 mA and the scan velocity around the standard working conditions of the ARCAM machine (~ 2000 mm s^{-1}).

Figure 1 shows the schematic of the TD-LAS optical arrangements used in this work. The TD-LAS recorded signal comes from a series of electron beam scans passing through (orthogonal to, see Fig. 2(a)) the laser beam. The Ti atoms evaporate from a Ti-6Al-4V bare substrate. For a detailed description of this experimental setup, the reader is referred to el Farsy *et al*.[23]. A tuneable solid laser diode emitting around 398.2 nm (Toptica Phototonics DL100, 15 mW maximum power and 3 mm beam diameter) was the laser source for absorption measurements. It probes the ground state of titanium atoms at λ_0 = 398.176 nm. This wavelength corresponds to the energy gap from the ground state $3d^2 4s^2$ to the upper excited state $3d^2(^3F)4s4p(^1P°)$ [25,26].

In the E-PBF process, the temperature variation of the melt pool is around 10^6 K s^{-1} because the electron beam scanning speed is around 2 m s^{-1}. So, the study of fusion dynamics requires measurement with a temporal resolution of 1 µs (acquisition frequency of ~1 MHz). For the TD-LAS measurements carried out in our previous work, the laser diode scanned the wavelength around λ_0 to measure Doppler broadening of evaporated atoms.[23] In that work, the acquisition frequency was about 80 Hz. To increase the temporal resolution of TD-LAS, we fixed in the present work the current injected into the laser diode, which has, as a consequence, kept constant the wavelength emitted by the laser (λ_0= 398.176 nm; spectral resolution $\Delta\lambda$ ~ 0.1 pm). Hence, the time resolution highly improves. However, only a fraction of evaporated atoms can be probed, the ones having the velocity component null with respect to the laser direction (v_y) and whatever the other components (v_x and v_z) are. The measured evaporated atoms are those having v_y <40 m s^{-1}, so low compared to the thermal velocity of evaporated atoms with 2000 K temperature (v_{th}~ 550m s^{-1}).

Remember, the electron beam spot diameter is about 200 µm, and the morphology variation of the molten pool is below this spot size. The spot size dictates a spatial resolution lower than 200 µm. Therefore, an optical fiber of 100 µm core diameter collects the laser beam transmitted intensity (figure 1). The selected volume of vapor using this detection system corresponds to a thin cylinder with a 100 µm diameter along the laser path, aligned with the *Y* axis. The recorded signal by the photodiode contains the contribution of the plasma emission created during the melting and laser photon (I_t). We observed that the plasma contribution and the scattering of the laser are negligible, then the absorbance writes as follows:

$$A = -\ln(I_t/I_0) \quad (1)$$

where I_t is the beam laser intensity after crossing the vapor/plasma, which follows the beer–Lambert law:

$$I_t = I_0 e^{-k_{\lambda_0} L} \quad (2)$$

where I_0 is the laser intensity in the absence of the electron beam, $k_{\lambda 0}$ is the linear absorption coefficient for the wavelength λ_0, and L is the absorption length.

Figure 2 (b) shows a typically recorded signal of transmitted laser intensity and the obtained absorbance during melting the surface of 3 mm × 60 mm, as shown in figure 2 (a). In figure 2, each peak in the

transmitted laser signal or the absorbance corresponds to a single track of electron beam scan. We used a simple mono-directional hatching strategy for melting.

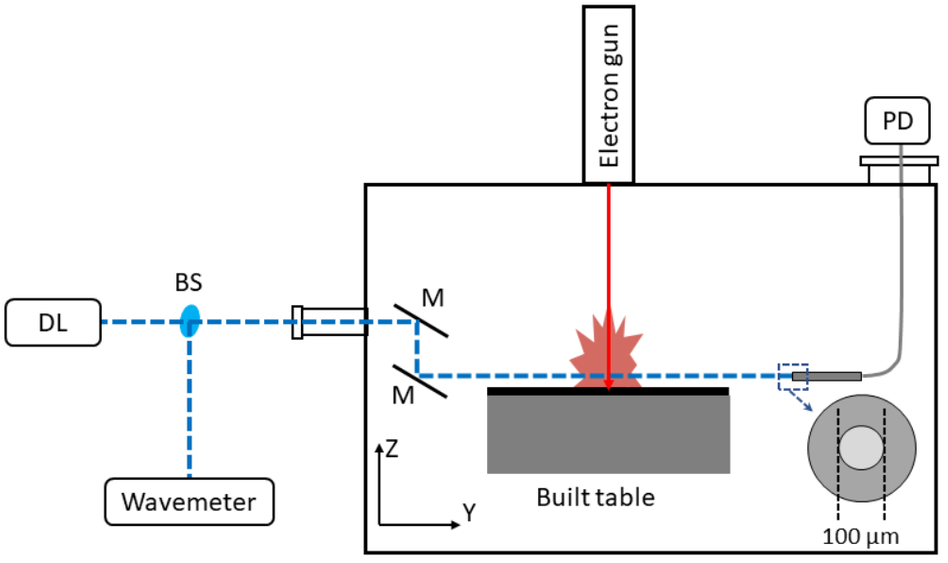

Figure 1. TD-LAS experimental setup used for the investigation of Ti evaporation in E-PBF (DL – diode laser, PD – photodiode, BS – beam splitter, M – mirror). The inset shows the detailed sketch of the optical fiber in cross section, with 100µm core diameter.

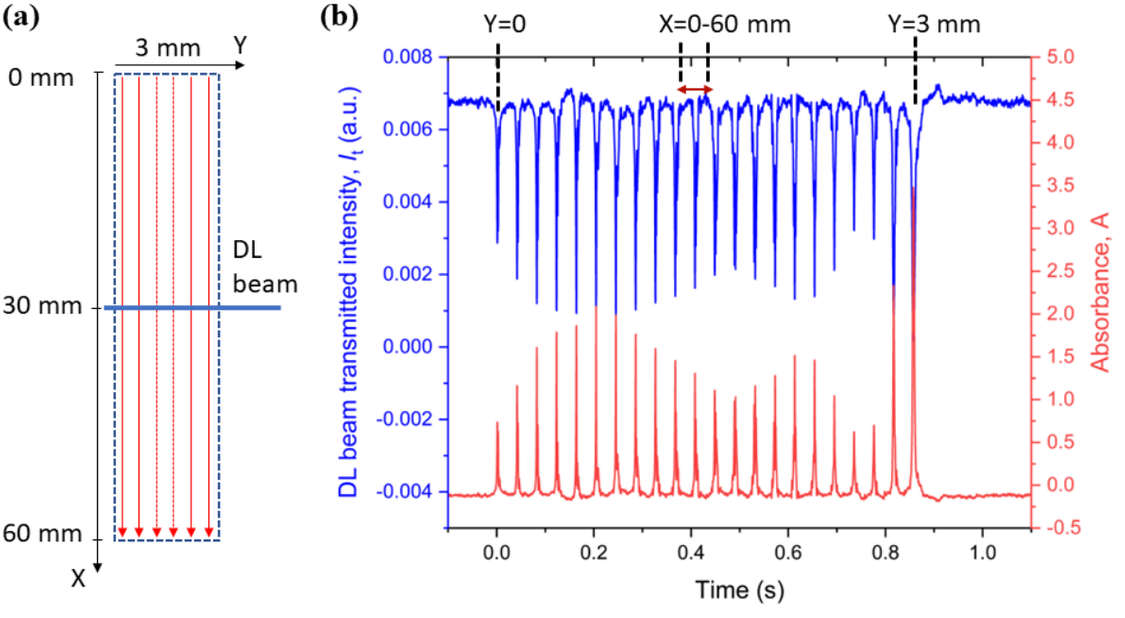

Figure 2. (a) The used hatching strategy to cover a surface of 3 mm × 60 mm. Top view. The blue horizontal line (at X = 30 mm) corresponds to the Diode Laser (DL) beam direction. (b) DL beam transmitted intensity and the absorbance ($-\ln(I_t/I_0)$ measured during the complete melting of the surface, each peak in curve correspond to a single track hatching in figure (a). I_0 is the average of transmitted intensity at [0.95, 1.05 s] in figure (b). The current intensity and the scan speed of the electron beam were 6 mA and 1000 mm s^{-1}, respectively.

III. Result and discussion

III-1. Absorbance fluctuations

To study the influence of the electron beam parameters, we performed measurements near the molten pool surface at the distance Z = 2 mm at different electron beam current intensities and scan speeds. Figure 3 shows the results of single-track hatching. Panel (a) of figure 3 shows the absorbance signal for a single track during the melting for different electron beam current intensities, while the panel (b) shows the absorbance for different scan speed of the electron beam. The space scale is the division of the scan speed by the time interval recorded on the oscilloscope. The maximum absorbance signal must correspond to the interaction between the electron beam and the molten pool, *i.e*., at X = 30 mm, because the beam laser path passes above the symmetry axis of the pool. This is illustrated by the case B in figure 3 (c), this point is used to calibrate the time scale acquired on the oscilloscope and determine the relative position between the electron beam interaction from the laser path. The titanium vapor plume is denser and more diffuse as the current intensity of the beam increases. The same behavior follows when the scan speed of the electron beam decreases (figure 3 (b)), with a constant current intensity (6 mA).

Analyzing the results reported in figure 3, one can observe a significant fraction of the evaporated atoms diffusing forward (X <30 mm) and backward (X >30 mm), *i.e*., preceding or following the molten pool. Notice that more atoms diffuse in backward of the molten pool. This could be easily explained by the liquid tail of the melt pool that follows the electron beam–material interaction. The most surprising result herein is the presence of severe fluctuations of the absorbance signal in the back of the molten pool. These fluctuations are independent of the electron beam current intensity and the scan speed. Measurements were also carried out with a fast scan direction reversed, i.e., the electron beam scan was -X direction and at different Ti-6Al-4V bare substrates, the result is alike the forward scan direction. They have the same shape, whatever the power and the linear energy of the electron beam are. Then, these oscillations seem related to the molten pool dynamics.

Many physical processes could be the origin creating those oscillations on the evaporated atoms. Several possible explanations virtually hold.

- Photon scattering with the electron beam: the electron beam which melts the material crosses the transmitted laser beam. During this interaction, electrons can scatter a fraction of the laser photons out of the beam. The consequence is an overestimation of the absorbance. The presence of several peaks in the recorded signal suggests an eventual multiple electron beam, containing quite a few spots[27], the laser intercepting them one by one during the scan track. However, the electron beam shape has been characterized (figure 4), and the electron beam is well focused, with only one spot, whatever the current intensity and scan speed are. Therefore, the measured signal allows us to rule out this hypothesis. In addition, measurements away from the substrate surface (Z > 50 mm) did not show those fluctuations.

- Spatter (large liquid droplets) intercepts the laser beam. They often travel towards the front of the molten pool as reported in selective laser powder bed fusion AM. Khairallah *et al*.[8] used

their high-fidelity multiphysics model to study the interaction of the laser beam with the sputter artificially introduced in front of the liquid pool. The simulations reveal the spatial-temporal detail of the sputter dynamic. With a 300-W laser at a scan speed of 1800 mm s^{-1} interacting with a large spatter suspended 40 µm above the powder bed, they show that the spatter is expelled away to the side of the melt pool with a velocity of 5000 mm s^{-1} in a time interval of 40 µs. The driven force is the vapor recoil pressure which exponentially increases with the temperature and creates the necessary impulse force. A similar process can appear in E-PBF. Regarding our measurements, these spatters could interfere with the laser leading to an overestimation of the absorbance signal. However, the observed fluctuations of the evaporated atoms are in the back-side of the molten pool (see Fig. 3(c)). Moreover, the repetition of the absorption patterns for several e-beam currents (Fig. 3(a)) and scan speeds (Fig. 3(b)) invalidates this assumption. Indeed, the spatter ejection is random. In addition, the vapor recoil pressure previously measured (~ 1 – 10 Pa)[23] seems weak to accelerate such a spatter. Furthermore, when the laser was detuned from the absorption transition λ_0 there were no fluctuations on the transmittance signal confirming that the spatters do not intercept the laser beam.

- The generation of big back-spatter (~200 µm) from the molten pool was found *via* modeling and *in situ* X-ray analysis.[8] Those spatter can arise in different AM processes and present major problems because they are oversized. Changes in the electron beam power during the melting result in a significant temperature change in the liquid pool surface. When the temperature increases, this leads to an exponential growth of the vapor recoil pressure. The vapor flow can generate the back spatter if the recoil pressure overcomes the surface tension. Khairallah *et al.*[8] defined a critical velocity to explain and prevent the production of high-speed backflow-induced spatters. These back spatters can explain the fluctuations in the density of evaporated atoms. They can result in hiding the evaporated volume from the electron beam–material interaction (vapor source) or interfering with the diagnostic laser beam. Those give respectively an underestimated and overestimated measurement. However, the regularity of the fluctuations and the similar pattern of low and high current tends to refute this possibility.

- Molten pool surface fluctuations are well-known. Scharowsky *et al*.[7] used a fast imaging device to observe the E–PBF on an Arcam A2 system with a very low electron beam scanning speed of 160 mm s^{-1}. They chose this speed, approximating that the dynamic of the molten pool overcomes the dynamic due to electron beam scan speed. In their pictures, static and fluctuating reflections appear. Static reflections came from the solid surface with an angle relative to the light of sight of the camera. Fluctuating reflections indicate the presence of a liquid phase. Scharowsky *et al*. reported the oscillation frequency obtained by the inverse time of appearance of a reflection in the order of 1.5 kHz. Here reported TDLAS measurements were very close to the liquid pool (Z = 2 mm). If the keyhole is present, which is the major vapor source, the liquid fluctuation could induce fluctuations in the diffusion of the vapor backward the molten pool. On the one hand, in the previous study for electron beam intensity higher than 6 mA, we measured a slight variation in the vapor temperature, which is in thermal equilibrium with the liquid surface of the pool. The temperature variation is in the range of 5000 – 6000 K.[23] On the other hand, surface fluctuations depend mainly on surface tension and liquid viscosity.[7] Since

the surface temperature does not undergo significant variations (latent heat), we expect similar surface fluctuations, probably at the origin of the detected absorbance fluctuation.

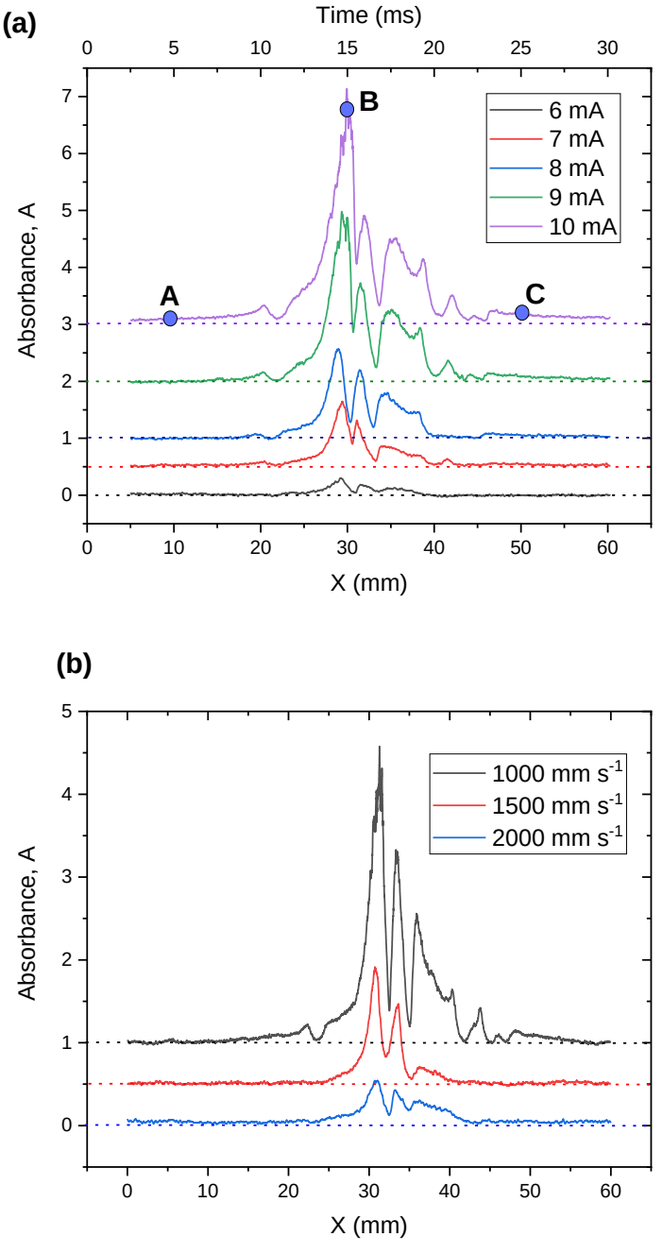

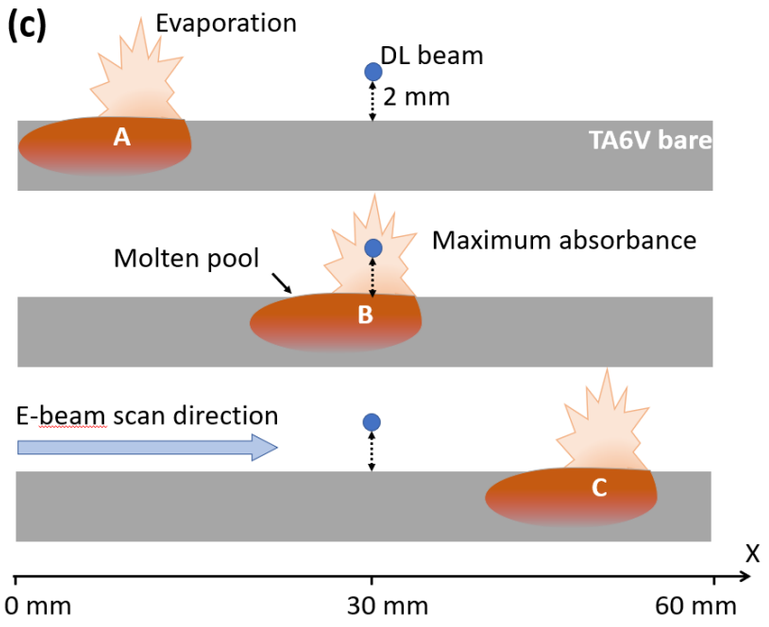

Figure 3. Absorbance signal for single-track hatching of 60 mm. (a) Measurements at different current intensities of the electron beam and fixed scan speed of 2000 mm s^{-1}. (b) Measurements at different scan speeds and fixed current intensity of the electron beam of 6 mA. (c) Sketch showning the corresponding molten pool position of the data A, B, and C in (a). The space scale comes from the product of the time recorded in the oscilloscope and the scan speed. We assumed that the maximum absorbance signal corresponds to X = 30 mm, where the molten pool should be as the laser beam intercepts the Ti vapor from under this location, position B. For clarity, the curves in (a) and (b) have been shifted, and the dashed line represents their base.

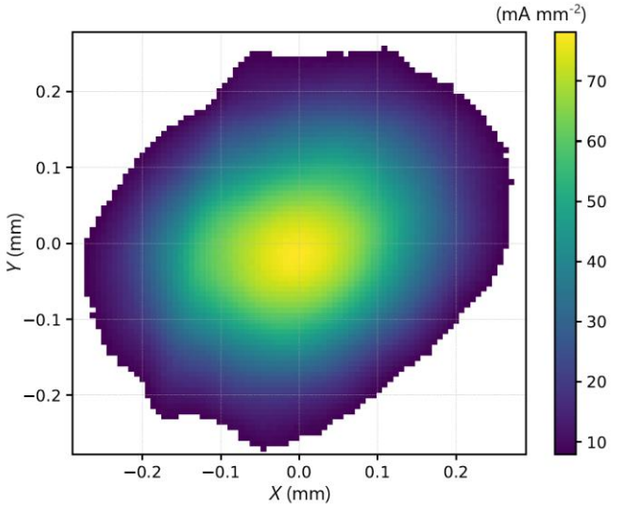

Figure 4. 2D current density of 8 mA electron beam spot.

III-2. Spatial distribution of the vapor

In this section, we present and discuss the measurements of the spatial distribution of the vapor plume in the plan (*XZ*). The plume reconstruction additions the measurements performed at different distances *Z* from the building surface. With respect to the previous set of measurements reported in Section III-1, here the diagnostic laser beam passes 2 – 30 mm above the building surface. The built table went down by steps of 2 mm keeping the laser fixed. Using this procedure, we obtained a matrix of the absorbance in the plan (*XZ*), shown in figure 5 and 6. Row data capture the signature of the fluctuations discussed in the previous sub-section (not shown). Hence, figure 5 and 6 present the averaged experimental data over all peak corresponding to melting of 3 × 60 cm^2 area, there are 22 single tracks hatching as shown in figure 2 (b).

In addition, we used the previous absolute measurements (Doppler profile)[23] carried on the same device to calibrate the relative absorbance measured at Z = 7 cm. Figures 5 and 6 show the 2D maps of the vapor space distribution during the melting at different electron beam current intensities and two fixed scan speeds of 2000 mm s^{-1} and 4000 mm s^{-1}, respectively. For both scan speeds, the absorbance signal shows a non-linear behavior of the absolute vapor density with the current intensity. The maximum increases by almost one decade, from 0.5 × 10^{15} cm^{-3} to 3.2 × 10^{15} cm^{-3}, while the current intensity of the beam rises only from 6 mA to 10 mA, at 2000 mm s^{-1} (figure 5). The same behavior occurs at a higher scan velocity of 4000 mm s^{-1} (figure 6). The evaporation is known to evolve exponentially as a function of the target temperature representing heat dissipation.[28] The present measurements undoubtedly show that the evaporated atom density depends directly on electron beam current intensity and less of the linear energy ($E_l = \frac{beam\ power}{scan\ speed}$). We observe a vapor density of 0.8 × 10^{15} cm^{-3} for the couple e-beam current / scan speed of 10 mA / 4000 mm s^{-1} which is significantly higher than 0.5 × 10^{15} cm^{-3} obtained at 6 mA / 2000 mm s^{-1} even if the linear energy is lower in the first case. This indicates that the heat dissipation by thermal conductivity in the liquid and solid state (powder and solid part) is not sufficient to evacuate the energy of the electron beam. Consequently, an overconcentration of the energy atop the liquid surface provokes higher evaporation and can also create a plasma. An efficient (optimal) energy transfer to the target (the material) seems performed at moderate current intensity. One should keep in mind that we measured only the Ti evaporation, other elements coexist in TA6V alloy and can be evaporated, especially Al which has a lower melting point.

Concerning the vapor plume shapes, at 2000 mm s^{-1}, different typical signatures appear line in figure 5: narrow ellipse shape (plume jet) at 6 mA, (reversed) tear shape at 8 mA, and oval shape at 10 mA. The plume shape evolves as a function of the current intensity (beam power) and seems to reflect the interaction regime of the electron beam with the melted surface: keyhole formation, plasma formation, melt pool surface size, Marangoni effect due to the surface temperature gradient. At 4000 mm s^{-1}, the e-beam current intensity was high (> 10 mA), and the vapor plume always had an oval shape (figure 6). One expects a similar vapor plume shape for similar linear energy. For instance, let us compare the plume shapes at 6 mA/2000 mm s^{-1} and 10 mA/4000 mm s^{-1}. The keyhole seems present even at low current intensity (6 mA) and it is the plume jet source. The oval shape at high current intensity seems to indicate the presence of a plasma atop the molten surface that diffuses away from the liquid surface. Increasing the plasma/liquid interaction area, can explain the observed oval shape of the vapor plume.

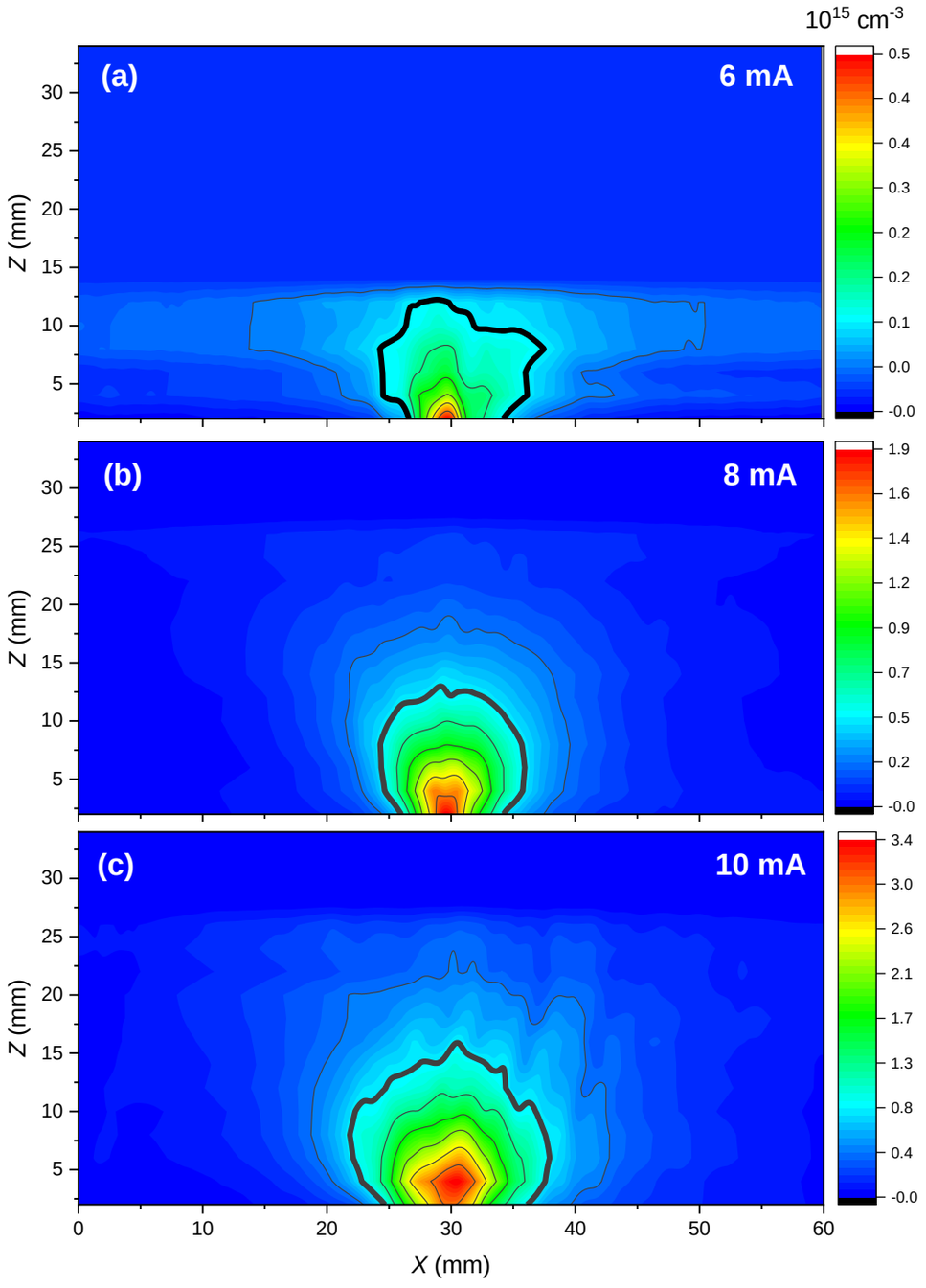

Figure 5: 2D vapor distribution at 2000 mm s^{-1} scan speed of the electron beam and a current intensity of 6 mA (a), 8 mA(b), and 10 mA (c). Data in figure are averaged over all peak shown in figure 2 (b). The absorption data without averaging at 10 mA and different Z are given in supplementary materials. The fluctuations appear in those data.

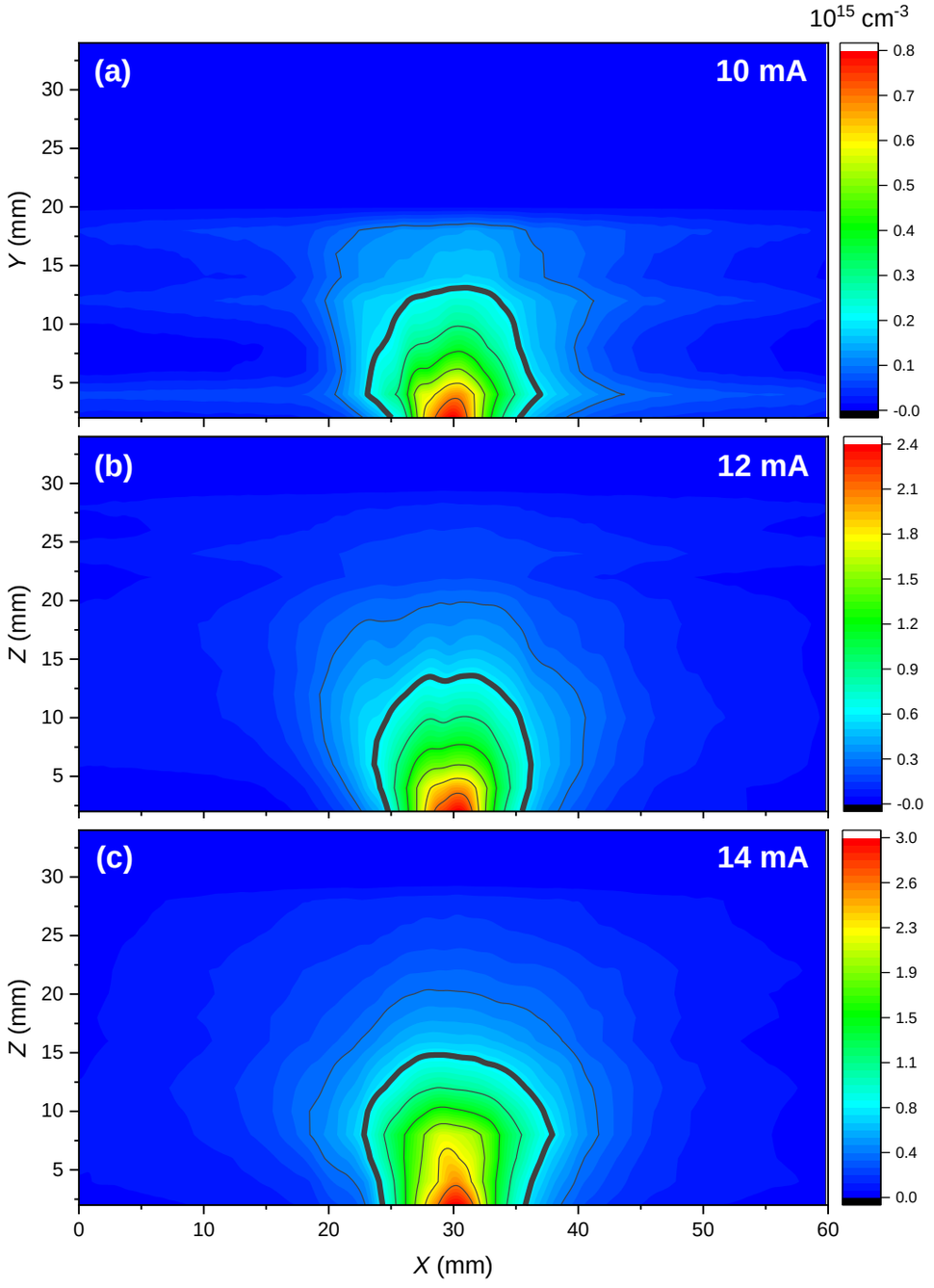

Figure 6. 2D vapor distribution at 4000 mm s^{-1} scan speed of the electron beam and a current intensity of 10 mA(a), 12 mA (b), and 14 mA (c). Data in figure are averaged over all peak shown in figure 2 (b).

IV. Conclusions

The tunable diode laser absorption spectroscopy (TD-LAS) allows *in-situ* characterization of the spatiotemporal variations of evaporated titanium atoms above the molten metal pool. The technique probes the ground state atoms during additive manufacturing by electron powder bed fusion (E-PBF). The high scan speed of the electron beam during melting produces pronounced temporal and thermal variations, allowing investigations at time resolutions down to the microsecond scale. In addition, well-focused beam spots (~200 µm) reliably produce smaller molten pools down to 50 µm in diameter.

Measurements performed under the standard operating conditions of the Arcam machine highlighted strong fluctuations in the evaporated metal that are independent of the electron beam power (current) and scan speed. These fluctuations probably arise from liquid surface dynamics. Our method revealed the shape of the vapor plume by adding the spatial profile of the vapor density measured at different distances from the molten surface. The plume shape depended on the beam current and scan speed. The plume was narrow and elongated at low currents, teardrop-shaped at average operating currents, and became ovoid at high currents. Finally, the total power transferred to the metal powder is the key external parameter determining optimal E-PBF melting conditions, whereas the linear energy density is only of secondary importance.

The measurements presented in this manuscript only contain a plan view, and aims as a proof of concept of the proposed laser diagnostic technique. It integrates the absorption signal through the direction perpendicular to the electron beam scan direction. Further works aims to synchronize the absorption signal with the current passing into the coils controlling the electron beam scan. The vapor plume can be re-constructed following several other plans (with different orientations relative the electron beam scan) and then a tomographic approach could be used to build the vapor plume in 3D.

Supplementary Material

The absorption data for a single-track hatching (i.e. without averaging as shown in figure 5c) at 10 mA electron beam current intensity and 2000 mm s^{-1} scan speed and all probed Z [2, 32 mm] are given in the attached excel file. The fluctuations appear in these data.

Acknowledgements

This work was performed in the framework of the SOFIA project supported by BPI France. The authors thank Dr. Quentin Vuillemin and Dr. Adrien Revel for the electron beam characterization.

Data Availability

The data that support the findings of this study are available from the corresponding author upon reasonable request.

References

[1] B. Vayre, F. Vignat, and F. Villeneuve, Mechanics & Industry **13**, 89 (2012).

[2] P.S. Cook and A.B. Murphy, Additive Manufacturing **31**, 100909 (2020).

[3] C. Körner, International Materials Reviews **61**, 361 (2016).

[4] L.E. Murr, Additive Manufacturing **5**, 40 (2015).

[5] L.E. Murr, S.M. Gaytan, D.A. Ramirez, E. Martinez, J. Hernandez, K.N. Amato, P.W. Shindo, F.R. Medina, and R.B. Wicker, Journal of Materials Science & Technology **28**, 1 (2012).

[6] P. Petrov, C. Georgiev, and G. Petrov, Vacuum **51**, 339 (1998).

[7] T. Scharowsky, F. Osmanlic, R.F. Singer, and C. Körner, Appl. Phys. A **114**, 1303 (2014).

[8] S.A. Khairallah, A.A. Martin, J.R.I. Lee, G. Guss, N.P. Calta, J.A. Hammons, M.H. Nielsen, K. Chaput, E. Schwalbach, M.N. Shah, M.G. Chapman, T.M. Willey, A.M. Rubenchik, A.T. Anderson, Y.M. Wang, M.J. Matthews, and W.E. King, Science **368**, 660 (2020).

[9] J.Y. Lee, S.H. Ko, D.F. Farson, and C.D. Yoo, J. Phys. D: Appl. Phys. **35**, 1570 (2002).

[10] Q. Chen, G. Guillemot, C.-A. Gandin, and M. Bellet, Additive Manufacturing **21**, 713 (2018).

[11] A. Klassen, T. Scharowsky, and C. Körner, J. Phys. D: Appl. Phys. **47**, 275303 (2014).

[12] T. Craeghs, S. Clijsters, Jean.-P. Kruth, F. Bechmann, and Marie.-C. Ebert, Physics Procedia **39**, 753 (2012).

[13] M. Islam, T. Purtonen, H. Piili, A. Salminen, and O. Nyrhilä, Physics Procedia **41**, 835 (2013).

[14] P.J. DePond, J.C. Fuller, S.A. Khairallah, J.R. Angus, G. Guss, M.J. Matthews, and A.A. Martin, Commun Mater **1**, 92 (2020).

[15] Y. Kawahito, N. Matsumoto, M. Mizutani, and S. Katayama, Science and Technology of Welding and Joining **13**, 744 (2008).

[16] C.S. Lough, L.I. Escano, M. Qu, C.C. Smith, R.G. Landers, D.A. Bristow, L. Chen, and E.C. Kinzel, Journal of Manufacturing Processes **53**, 336 (2020).

[17] C.B. Stutzman, A.R. Nassar, and E.W. Reutzel, Additive Manufacturing **21**, 333 (2018).

[18] Z. Szymanski, J. Kurzyna, and W. Kalita, J. Phys. D: Appl. Phys. **30**, 3153 (1997).

[19] N. Tomozeiu, Thin Solid Films **541**, 32 (2013).

[20] J. Posada, M. Jubault, A. Bousquet, E. Tomasella, and D. Lincot, Thin Solid Films **582**, 279 (2015).

[21] R. Junjuri, S.A. Rashkovskiy, and M.K. Gundawar, Physics of Plasmas **26**, 122107 (2019).

[22] D. Lacroix, G. Jeandel, and C. Boudot, Journal of Applied Physics **81**, 6599 (1997).

[23] A. el Farsy, V.G. Antunes, B. Seznec, L. Schiesko, C. Ballage, and T. Minea, Journal of Applied Physics **132**, 054904 (2022).

[24] B.J. Simonds, J.W. Sowards, and P.A. Williams, J. Phys. D: Appl. Phys. **50**, 325602 (2017).

[25] A.E. Farsy, J. Ledig, M. Desecures, J. Bougdira, and L. de Poucques, Plasma Sources Sci. Technol. **28**, 035005 (2019).

[26] A. Revel, A. El Farsy, L. de Poucques, J. Robert, and T.M. Minea, Plasma Sources Sci. Technol. (2021).

[27] J.W. Elmer, 13 (n.d.).

[28] V. Juechter, T. Scharowsky, R.F. Singer, and C. Körner, Acta Materialia **76**, 252 (2014).

AIP Publishing

Journal of Applied Physics

ACCEPTED MANUSCRIPT

This is the author's peer reviewed, accepted manuscript. However, the online version of record will be different from this version once it has been copyedited and typeset.
PLEASE CITE THIS ARTICLE AS DOI: 10.1063/5.0131102

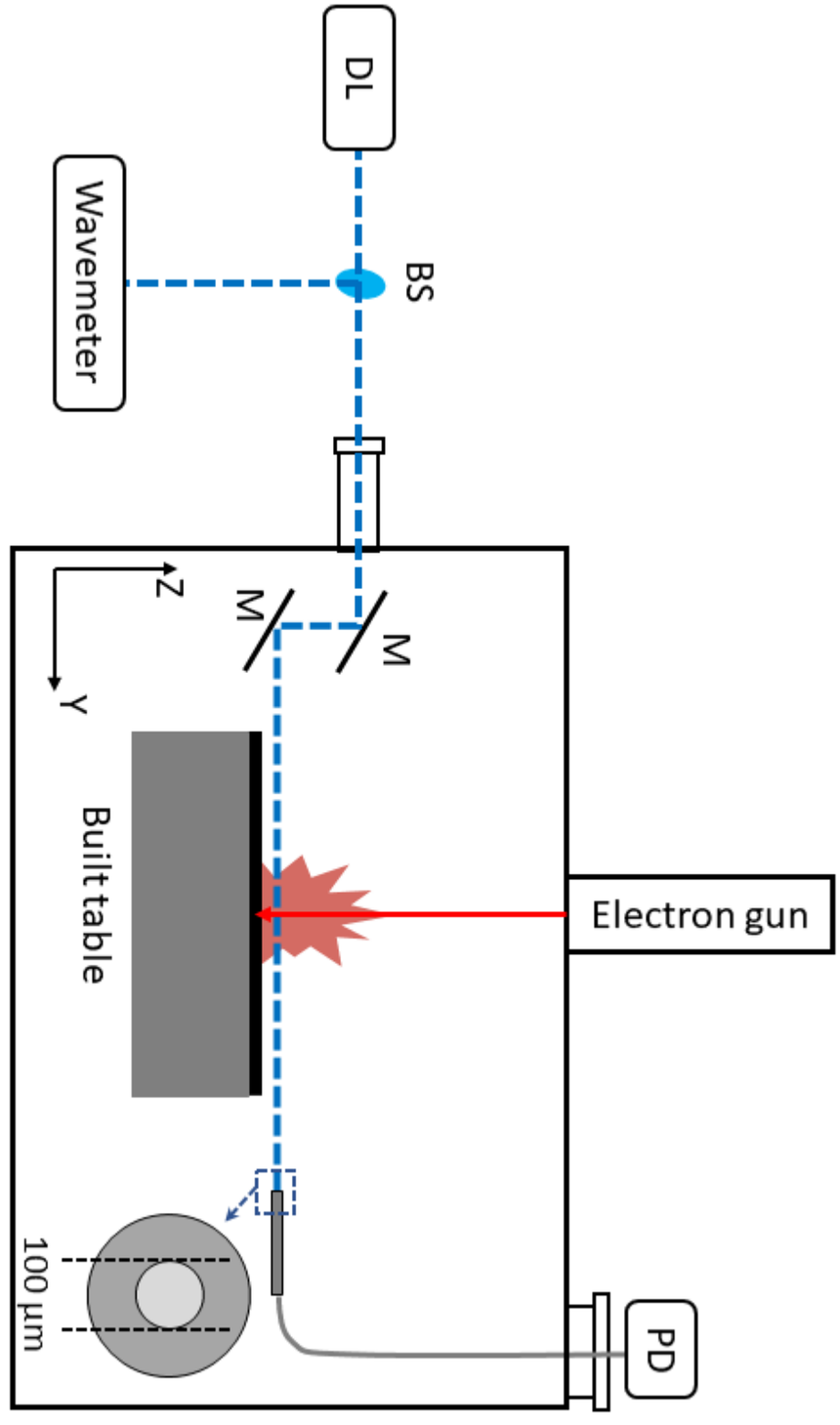

Journal of Applied Physics

AIP Publishing

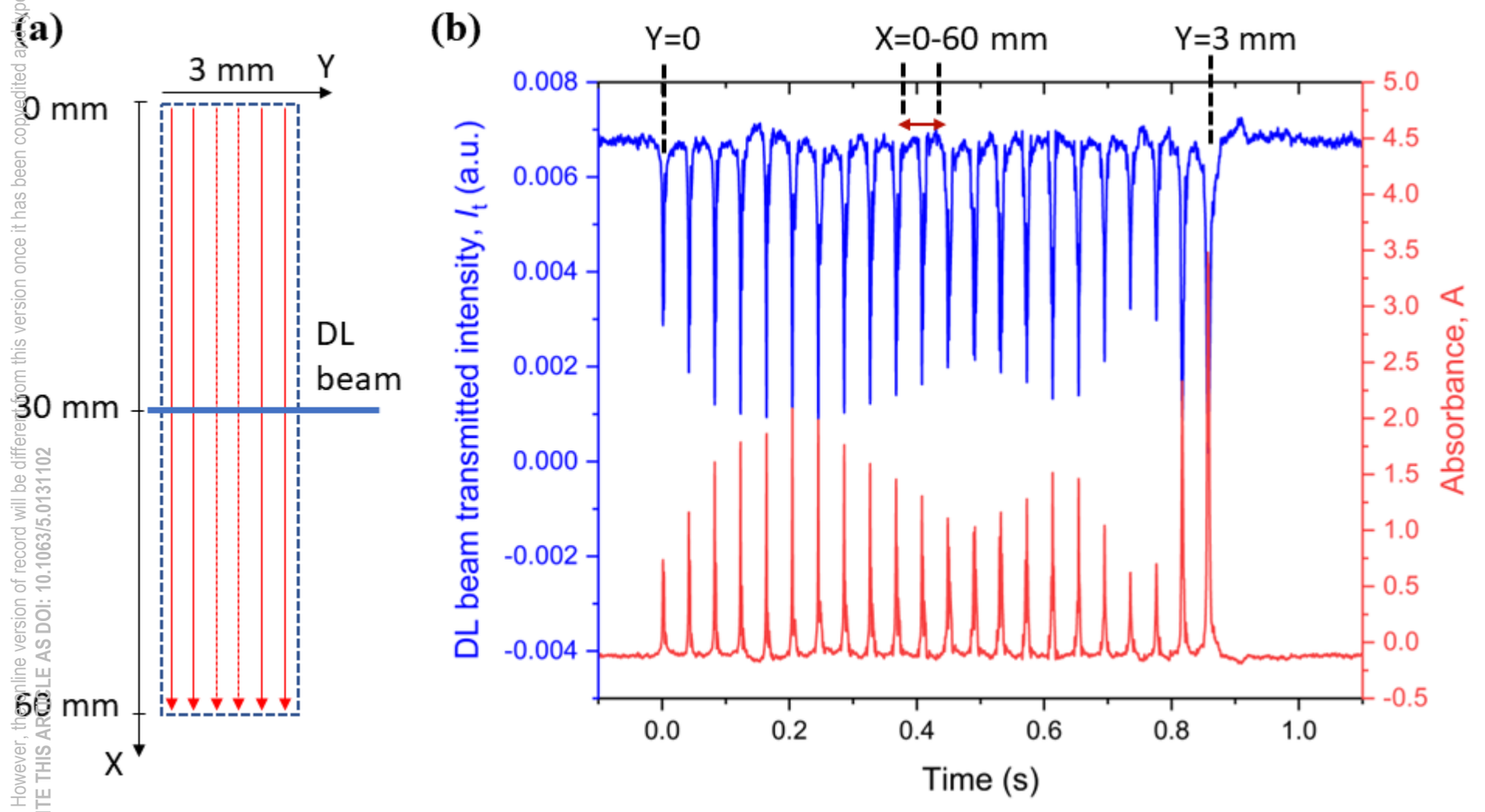

AIP Publishing

Journal of Applied Physics

ACCEPTED MANUSCRIPT

This is the author's peer reviewed, accepted manuscript. However, the online version of record will be different from this version once it has been copyedited and typeset.
PLEASE CITE THIS ARTICLE AS DOI: 10.1063/5.0131102

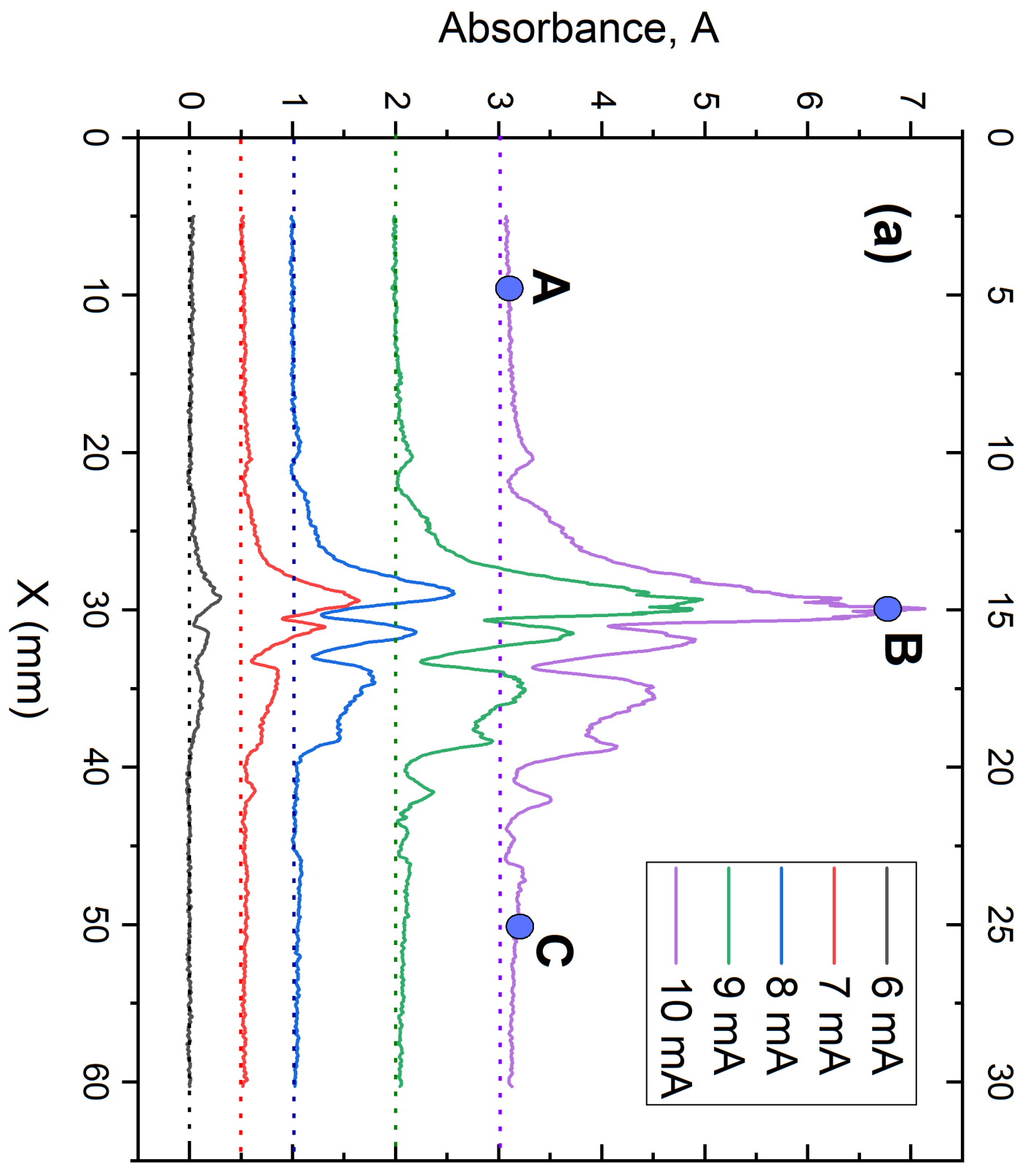

AIP Publishing

Journal of Applied Physics

ACCEPTED MANUSCRIPT

This is the author's peer reviewed, accepted manuscript. However, the online version of record will be different from this version once it has been copyedited and typeset.
PLEASE CITE THIS ARTICLE AS DOI: 10.1063/5.0131102

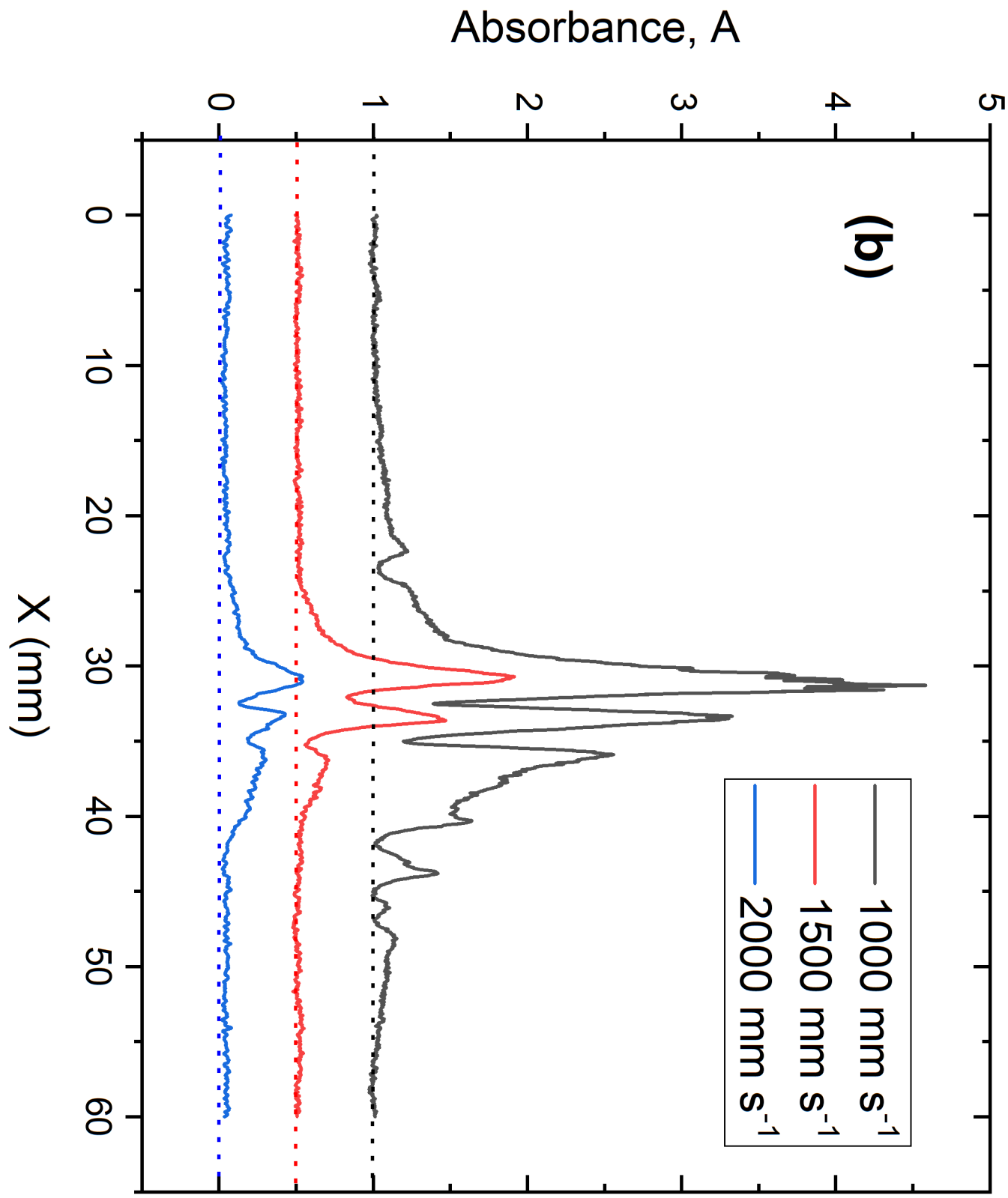

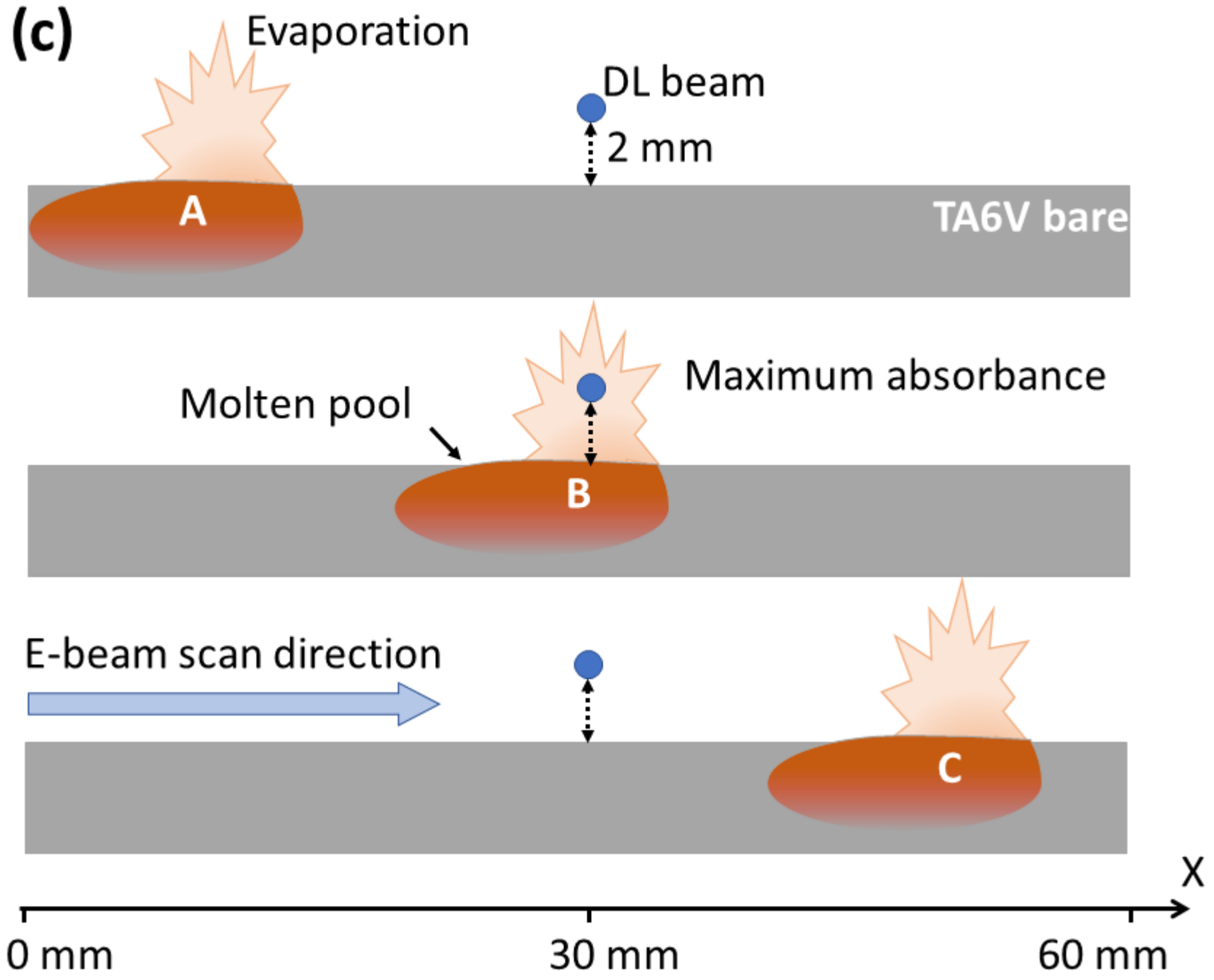

Journal of Applied Physics

AIP Publishing

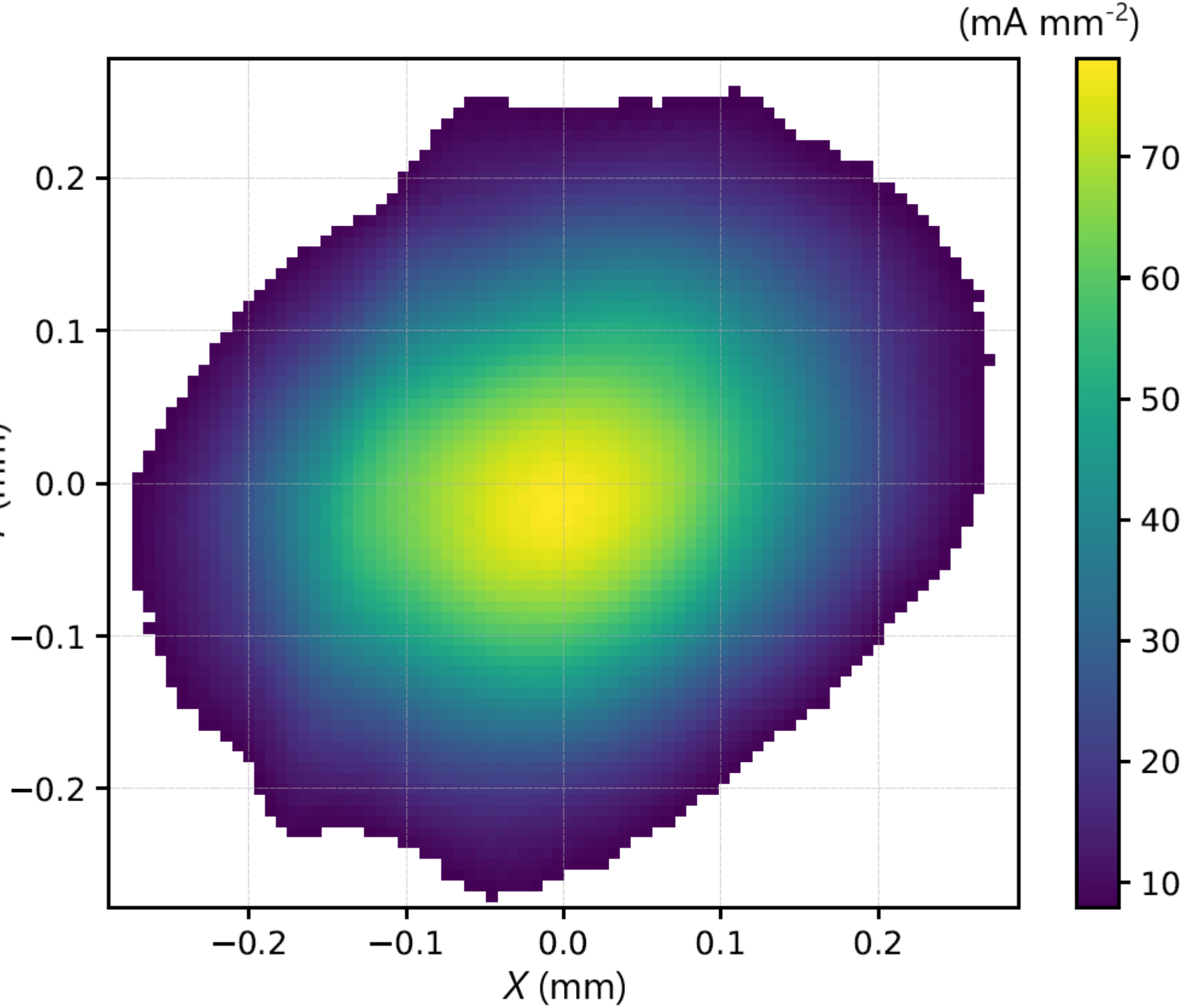

AIP Publishing

Journal of Applied Physics

ACCEPTED MANUSCRIPT

This is the author's peer reviewed, accepted manuscript. However, the online version of record will be different from this version once it has been copyedited and typeset.
PLEASE CITE THIS ARTICLE AS DOI: 10.1063/5.0131102

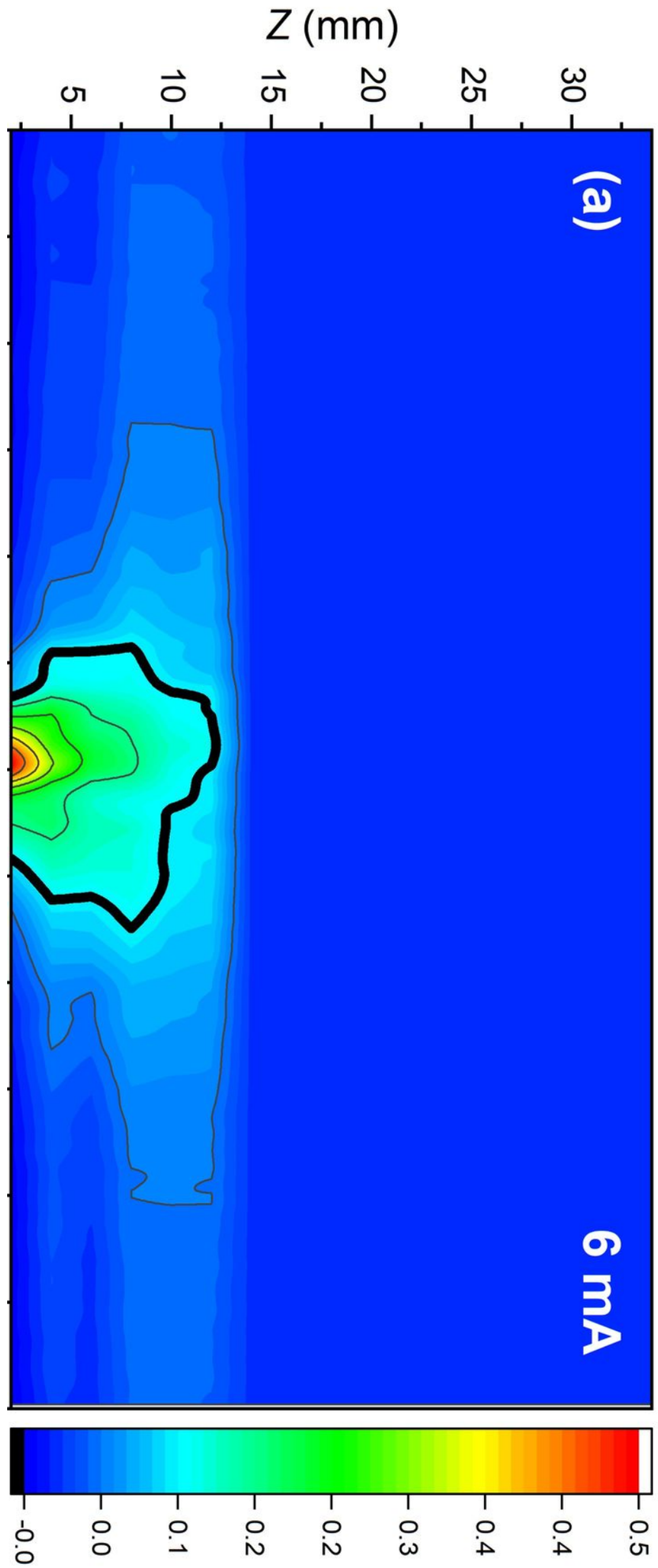

AIP Publishing

Journal of Applied Physics

ACCEPTED MANUSCRIPT

This is the author's peer reviewed, accepted manuscript. However, the online version of record will be different from this version once it has been copyedited and typeset.
PLEASE CITE THIS ARTICLE AS DOI: 10.1063/5.0131102

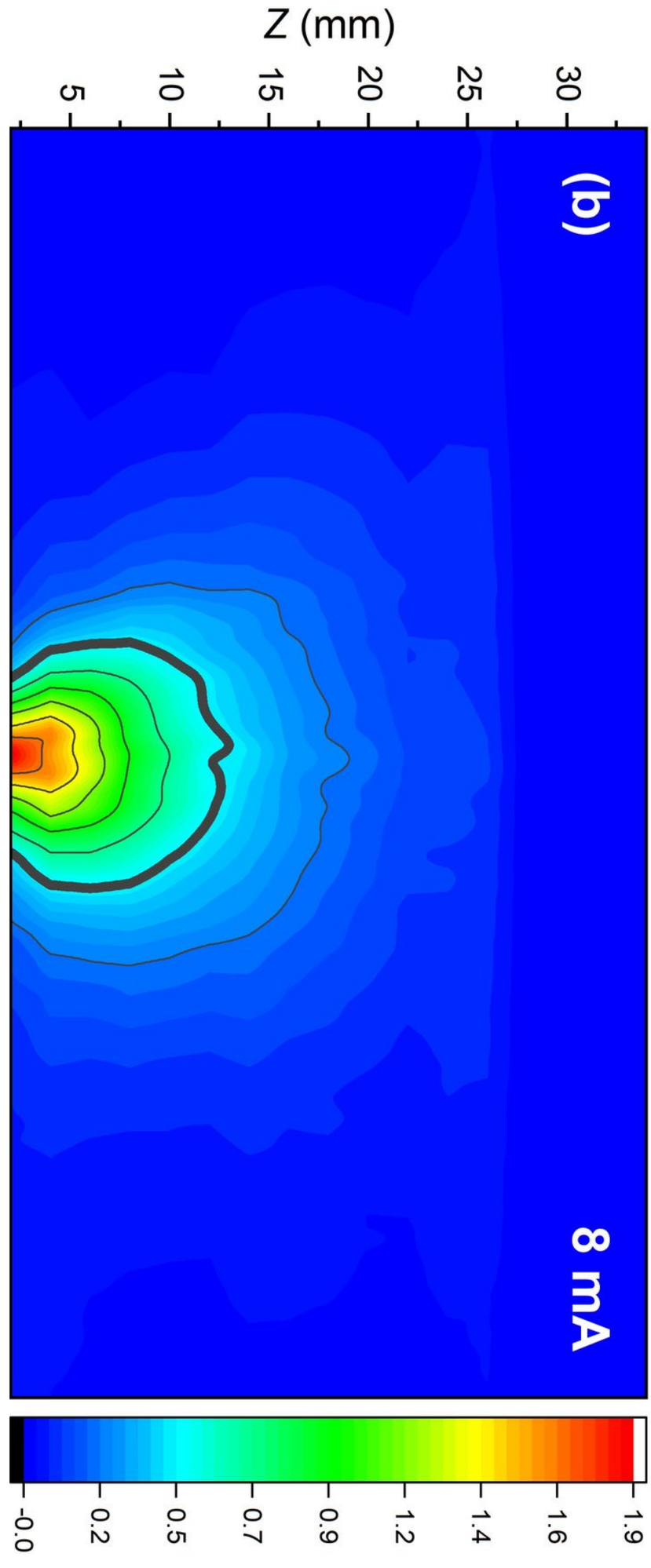

AIP Publishing

Journal of Applied Physics

ACCEPTED MANUSCRIPT

This is the author's peer reviewed, accepted manuscript. However, the online version of record will be different from this version once it has been copyedited and typeset.
PLEASE CITE THIS ARTICLE AS DOI: 10.1063/5.0131102

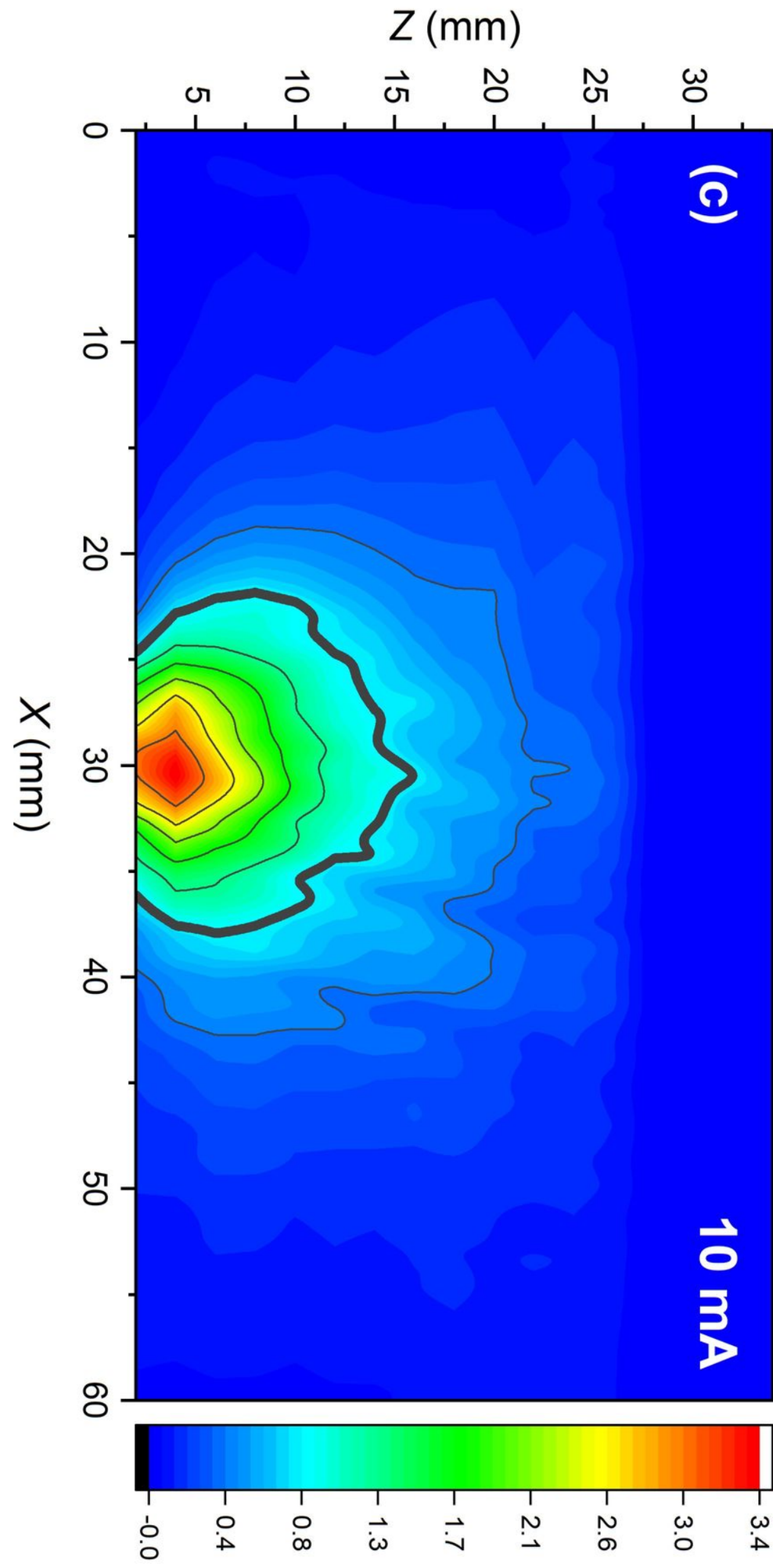

AIP Publishing

Journal of Applied Physics

ACCEPTED MANUSCRIPT

This is the author's peer reviewed, accepted manuscript. However, the online version of record will be different from this version once it has been copyedited and typeset.
PLEASE CITE THIS ARTICLE AS DOI: 10.1063/5.0131102

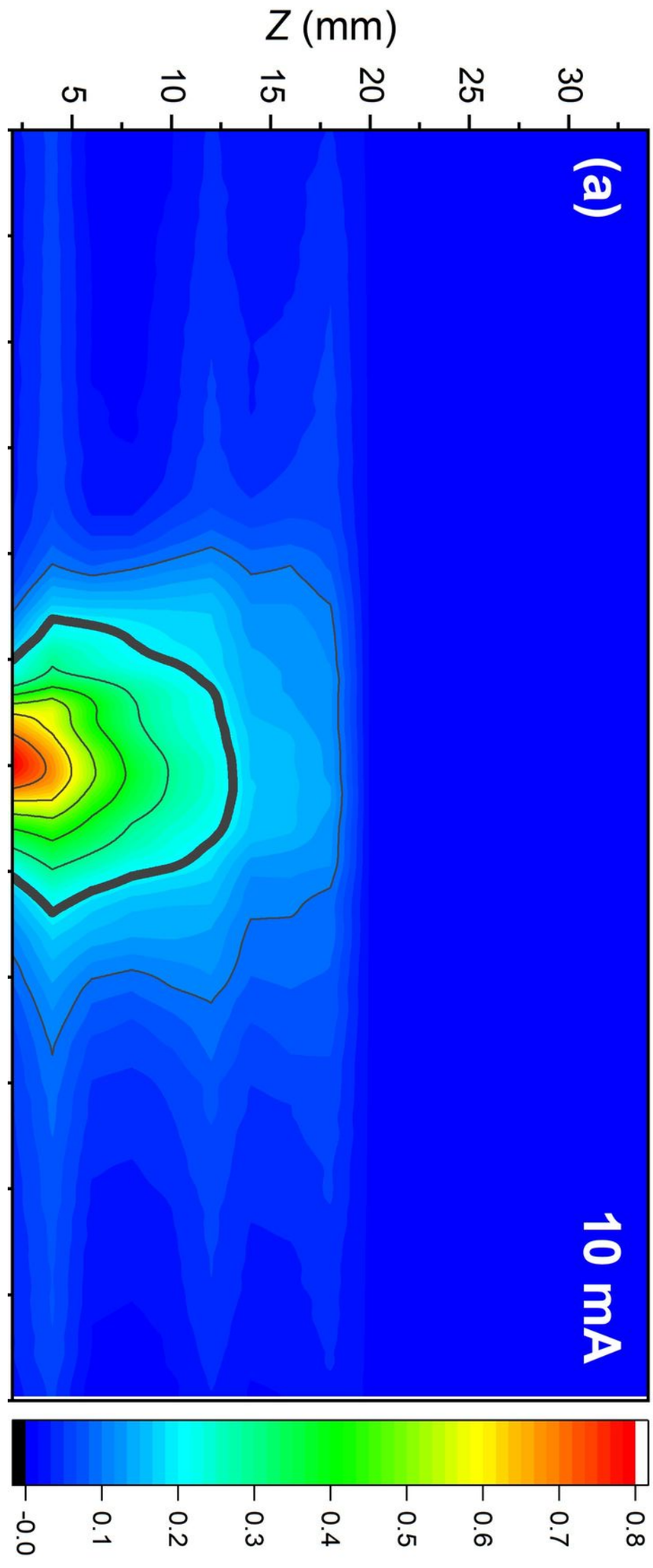

AIP Publishing

Journal of Applied Physics

ACCEPTED MANUSCRIPT

This is the author's peer reviewed, accepted manuscript. However, the online version of record will be different from this version once it has been copyedited and typeset.
PLEASE CITE THIS ARTICLE AS DOI: 10.1063/5.0131102

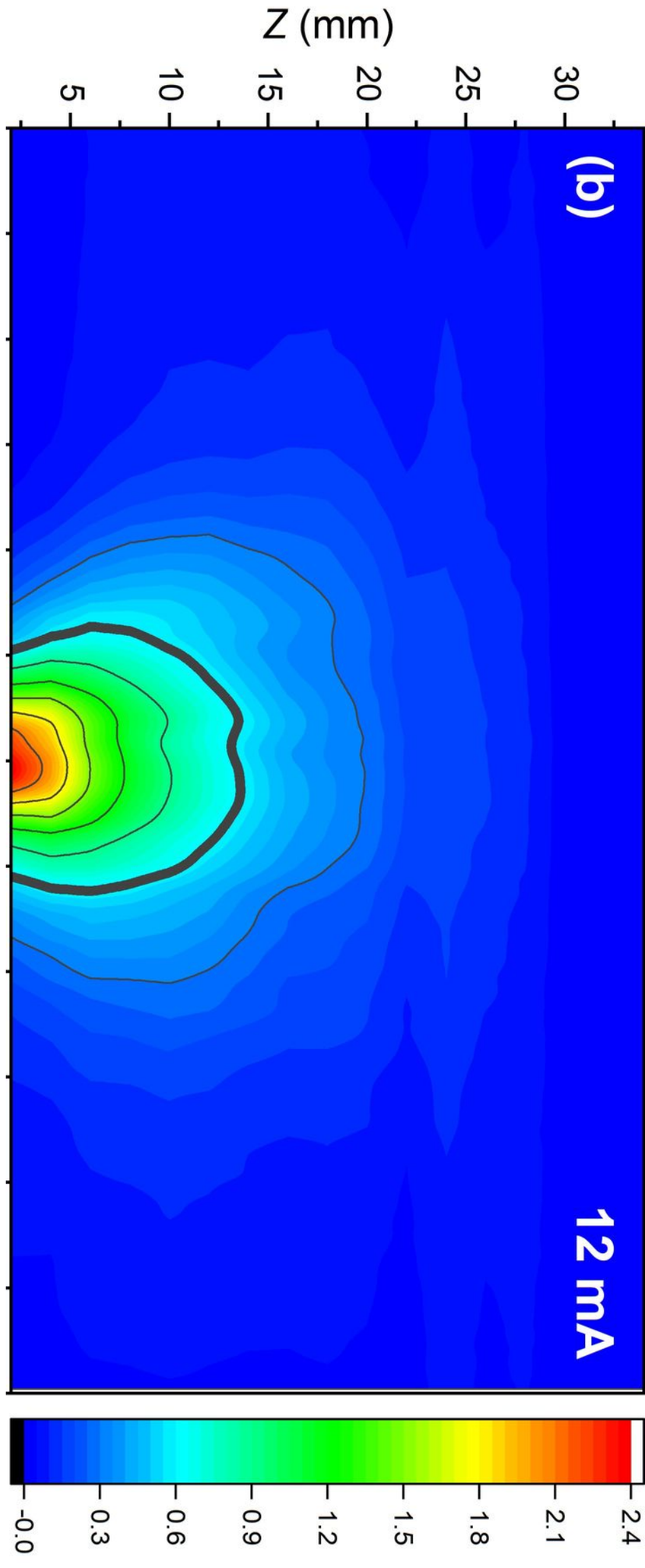

AIP Publishing

Journal of Applied Physics

ACCEPTED MANUSCRIPT

This is the author's peer reviewed, accepted manuscript. However, the online version of record will be different from this version once it has been copyedited and typeset.
PLEASE CITE THIS ARTICLE AS DOI: 10.1063/5.0131102